Available online at www.sciencedirect.com
ScienceDirect
Optics Communications 281 (2008) 210–216
OPTICS COMMUNICATIONS
www.elsevier.com/locate/optcom

Wavefront sensing based on rotated lateral shearing interferometry

M. Schwertner [1], M.J. Booth, T. Wilson *

Department of Engineering Science, University of Oxford, Parks Road, Oxford OX1 3PJ, UK

Received 28 May 2007; received in revised form 4 September 2007; accepted 7 September 2007

Abstract

We describe a self-referencing method of wavefront sensing based on rotated lateral shearing interferometry which is able to measure the local slope of a wavefront. We describe the principle of operation, suggest a number of practical implementations, and present experimental results. We found the difference between two sequential measurements of a nominally flat wavefront to be better than $\lambda/250$ root mean square.

1. Introduction

Since the measurement of the phase distribution of an optical beam is a key issue in many branches of optics many phase measurement methods have been developed. Direct interferometry [1] is perhaps the most common technique. It requires a reference wavefront and is often combined with phase shifting or fringe analysis. Shack–Hartmann wavefront sensors [2], on the other hand, are self referencing and can operate at very high frame rates. However, the spatial resolution is often rather low in this case, the dynamic range is fixed by the geometry of the lenslet array and increased spatial resolution requires expensive, high resolution CCDs. Classical shearing interferometry [3] is a self-referencing technique which can measure the gradient of the wavefront in two orthogonal directions simultaneously [4] or sequentially [3]. Typical implementations also use phase shifting. Alternatively rather than measuring the wavefront directly it is also possible to measure the modal (Zernike) content of the field [5].

The underlying idea of the rotated lateral shearing (RLS) method we are about to describe is to produce a series of shearing interferograms, where interferograms for different orientations of the (constant magnitude) shearing vector are recorded. If we rotate the direction of the shearing vector in a plane perpendicular to the optical axis, this leads to a temporal modulation of the interference pattern for each location within the beam, which then allows us to obtain the local gradient of the wavefront for each location.

2. Rotated lateral shearing interferometry

We wish to measure the phase $\phi(x, y)$ of the beam Ψ_1 which has an amplitude described by the real parameter A:

$$\Psi_1(x,y) = A\exp(\mathrm{j}\phi(x,y)). \tag{1}$$

In order to achieve this goal, we create a sheared version of this beam:

$$\Psi_2(x,y) = A\exp[\mathrm{j}(\phi(x+\Delta x, y+\Delta y)+\delta)], \tag{2}$$

where we have assumed that the amplitude does not vary significantly on the scale of the shearing distance. The vector $(\Delta x, \Delta y)$ describes the lateral displacement of the sheared beam in respect to the original beam and δ accounts for any constant phase offset between the two beams. The positive shearing distance, r, relates to its cartesian components via $r^2 = \Delta x^2 + \Delta y^2$.

We intend to measure the phase $\phi(x,y)$ via the local slope of the wavefront consisting of the components

* Corresponding author.
E-mail addresses: Michael.Schwertner@gmail.com (M. Schwertner), Tony.Wilson@eng.ox.ac.uk (T. Wilson).
[1] Present address: Carl Zeiss MicroImaging GmbH, Carl-Zeiss-Promenade 10, 07745 Jena, Germany.

0030-4018/$ - see front matter © 2007 Elsevier B.V. All rights reserved.
doi:10.1016/j.optcom.2007.09.025

$$s_x(x,y) = \frac{\partial}{\partial x}\phi(x,y) = S(x,y)\cos\alpha(x,y);$$
$$s_y(x,y) = \frac{\partial}{\partial y}\phi(x,y) = S(x,y)\sin\alpha(x,y), \tag{3}$$

where the angle $\alpha(x,y)$ describes the orientation of the normal vector of the wavefront and $S(x,y)$ is the magnitude of the slope vector. The measured array of slope values will later allow us to reconstruct the phase $\phi(x,y)$ itself. Now we make the shear vector $(\Delta x, \Delta y)$ follow a circular motion, which may be expressed as:

$$(\Delta x, \Delta y) = (r\cos\theta, r\sin\theta), \tag{4}$$

where r is the shear distance and the angle θ describes the orientation of the shearing vector in a plane perpendicular to the optical axis. If the shearing distance is relatively small, we may approximate the phase of the sheared beam in Eq. (2) with:

$$\begin{aligned}\phi(x+\Delta x, y+\Delta y, \theta) &\approx \phi(x,y) + \Delta x s_x + \Delta y s_y \\ &= \phi(x,y) + rS\cos(\theta-\alpha),\end{aligned} \tag{5}$$

where we have omitted the explicit dependence of α and S on (x,y) for brevity. We now examine the intensity pattern produced by the interference of the two beams:

$$\begin{aligned}I(x,y,\theta) &= |\Psi_1(x,y,\theta) + \Psi_2(x,y,\theta)|^2 \\ &= 2A^2[1+\cos(rS\cos(\theta-\alpha)+\delta)].\end{aligned} \tag{6}$$

The measurement principle is now clear: rotating the shearing vector (varying θ) leads to a local modulation of the detected interferogram intensity, depending on the shear orientation. This modulation contains information about the local slope of the wavefront. At this point it is important to note that the spatial structure of the detected interferogram (6) is not evaluated. This distinguishes the RLS method from fringe pattern analysis [6] and related approaches, where phase information is inferred from the spatial structure of the interferogram. For RLS, processing of the modulation recorded during subsequent measurement of a single pixel is sufficient to determine the local wavefront slope at the location of that pixel.

2.1. Several options for data processing

We will now discuss three different procedures that can be used to extract the local slope of the wavefront from the local modulation of the intensity. The choice of the procedure depends on the application. We will begin with the most general case of arbitrary phase differences between the two sheared beams. Here the phase offset δ (see Eq. (6)), can take any value thus relaxing requirements for optical component quality and/or alignment. We can rewrite Eq. (6) as

$$I(x,y,\theta) = 4A^2\left[\cos^2\left(\frac{\delta}{2} + \frac{rS(x,y)}{2}\cos(\theta-\alpha(x,y))\right)\right]. \tag{7}$$

We can fit the above equation to the measured series of interferograms, $I(x,y,\theta)$, in order to extract the parameters for the local slope, $S(x,y)$, and its orientation, $\alpha(x,y)$. Another point to mention is the ambiguity in α in case the parameter δ is zero or a multiple of π (see Eq. (7)). Then the angle α would be defined apart from a constant offset $n\pi$, where n is an integer. Therefore, it is advantageous to adjust δ to a value close to $\pi/2$ to avoid this ambiguity. Alternatively a way to resolve this ambiguity in α is to superimpose an overall constant tilt to the wavefront under test. This restricts the range of α and thus eliminates the problem at the expense of a slightly reduced sensitivity.

So far we have treated the associated data processing for arbitrary phase differences. If we design the system such that the phase differences between the two beams is in the range of approximately ± 0.5 radians, we can simplify our data analysis even further and speed up processing because nonlinear fitting is no longer required.

If we choose $\delta = \pi/2$ and note that $\cos(\pi/2+\epsilon) = -\sin\epsilon \approx -\epsilon$, i.e. the product of the local slope $S(x,y)$ and the shearing distance r in the argument of the sine function is small, we find from (6):

$$I(x,y,\theta) = 2A^2[1 - rS(x,y)\cos(\theta-\alpha(x,y))]. \tag{8}$$

From the above equation we see that for each location (x,y) the measured function $I(x,y,\theta)$ represents a sinosodially modulated signal. It is now straightforward to extract the parameters $\alpha(x,y)$ and the product rS (x,y) from the signal using, for example, Fourier techniques. Algorithms as well as a treatment of the related errors can be found for example in [7]. If the shearing distance r is known from the design or has been calibrated it is then a simple matter to obtain $S(x,y)$. It is also noted that a slight violation of the restriction made to the total modulation of the phase difference or an inaccuracy in $\delta = \pi/2$ can be tolerated if the Fourier processing extracts the modulation and phase of the fundamental frequency while rejecting higher harmonics.

A third and very interesting method to recover the slope data was pointed out by a referee, uses synchronous processing and is also outlined in [8]. We rewrite Eq. (6) to obtain:

$$\begin{aligned}I(x,y,\theta) = 2A^2[1 &+ \cos(rS\cos(\theta-\alpha)\cos\delta \\ &- \sin(rS\cos\theta-\alpha)\sin\delta)].\end{aligned} \tag{9}$$

To simplify our example we treat the special case where $\delta = \pi/2$ and yield

$$I(x,y,\theta) = 2A^2[1 - \sin(rS\cos\theta)\cos\alpha + \cos(rS\cos\theta)\sin\alpha]. \tag{10}$$

Some terms in the above equation can be expanded into a series [9]:

$$\cos(rS\cos\theta) = J_0(rS) + 2\sum_{k=1}^{\infty}(-1)^k J_{2k}(rS)\sin[(2k+1)\theta],$$
$$\sin(rS\cos\theta) = 2\sum_{k=0}^{\infty}(-1)^k J_{2k+1}(rS)\cos[(2k+1)\theta], \tag{11}$$

where $J_k(\cdot)$ denotes the Bessel function of the first kind and order k. The angle θ represents the shearing orientation, which is rotated during the process: ($\theta = \omega t$) and intensity images are recorded for a number of orientations θ such that the interval [0, 2π] is covered with equidistant steps. When Eq. (11) are inserted into (10), averaging over the product with $\sin(3\omega t)$ and $\cos\omega t$ leaves:

$$\begin{aligned}\langle I(x,y,\omega t)\sin(3\omega t)\rangle &= 2A^2[J_2(rS)\sin\alpha],\\ \langle I(x,y,\omega t)\cos(\omega t)\rangle &= 2A^2[J_1(rS)\cos\alpha].\end{aligned} \tag{12}$$

Here we made use of the orthogonality relationship and $\langle\cdot\rangle$ denotes averaging over an integer number of periods. This set of two Eqs. (12) contains the two unknown variables for the magnitude of the tilt, S, and the tilt orientation, α. The shearing distance r is known from the properties of the setup or a calibration procedure. Solving the above set of equations numerically leads to the phase gradients values for every pixel. Because the Bessel functions J_1 and J_2 oscillate, the total phase difference rS, which appears as the argument of the Bessel functions, has to be in the range before the first maximum of J_1, e.g. $rS \leqslant 1.5$ radians, to avoid ambiguities. Note that this range is larger than the range of the linear method.

After applying one of the above methods one obtains an array of phase slope measurements covering the entire wavefront. The next step is the reconstruction of the wavefront itself from this data. There are many approaches which can be taken here, for example [10–14]. These methods aim to minimise the error of the reconstructed wavefront. However, the simple but less robust method of direct integration can be used to reconstruct the wavefront and will be explained in the experimental section.

3. Practical implementations

Fig. 1 shows several options for the construction of a device where the magnitude of the shearing vector is constant but its orientation can be rotated in a plane perpendicular to the optical axis.

In (a) a birefringent image separation crystal is combined with a linear polariser into a rotating unit. This device is compact and the phase difference δ is determined by the dimensions of the crystal. Unfortunately it is wavelength dependent and the shear distance and hence the sensitivity are not variable. Part (b) of Fig. 1 depicts an implementation based on Ronchi gratings where the shear can be varied by changing the distance d between the gratings. Details of the design and properties of a grating-based lateral shearing interferometer with phase stepping are described in [15,3]. The next implementation, (c), is essentially a Mach–Zehnder interferometer. A slightly tilted parallel plate is rotated around an axis parallel to the propagation direction of the incoming beam. This tumbling motion creates the required lateral shear of constant magnitude with rotating orientation. The lateral shear distance is determined by the tilt angle γ between the surface normal of the plate and the optical axis. This device can operate at different wavelengths.

Finally, the design shown in Fig. 1d combines two birefringent Wollaston prisms and a polariser into one rotating unit. A change of the distance d sets the shearing distance while a vertical translation of the second prism (not illustrated in the figure) allows the adjustment of the phase difference δ between the sheared beams. This design can also be used with different wavelengths if the quarter wave plate is chosen accordingly or one of an achromatic type is used.

4. Experimental

4.1. Setup

In this section we describe experimental results obtained with an implementation of the scheme shown in Fig. 1d. Fig. 2 shows a photograph of the rotating system. In order to demonstrate rotated lateral shearing interferometry we chose to implement data processing for arbitrary phase differences and used a superimposed tilt. It should be mentioned that, for this first proof of principle, we have built an optical system from components that were available in the laboratory. The specifications of the Wollaston prisms caused an undesirably large value of the shearing distance r and hence the product $r|S|$ such that the full expression for the interference pattern, Eq. (6), had to be used in the nonlinear fit.

4.2. Number of sampled shear orientations

As we can read from Eq. (7) the model has five unknown variables. Hence the theoretical minimum of required shearing orientations is five. However, since several oscillations of the fitted function may occur in case of large wavefront tilt, it is advantageous to sample a larger number of data points for the nonlinear fit. This also helps to reduce the influence of measurement noise. For our first experiments a total of 72 interferograms were captured to record one full cycle of the rotation of the shearing vector in steps of 5°. This is clearly an over-sampling of the modulated intensity and helps to reduce measurement noise. We chose this configuration to demonstrate the interesting ability of the new design to combine low-cost construction with precision, low noise measurement. In our first experiments the goniometer was adjusted manually. A data acquisition for 72 frames would take about 3 s within an automated setup at video frame rate and could be reduced significantly by faster image acquisition. Modern low-cost cameras with digital interface can deliver frame rates in the order of several hundred Hertz in case pixel binning is used or a region of interest (ROI) of the detector chip is read out only.

It has to be mentioned here that the required number of interferograms, the signal to noise properties as well as the computational effort are completely different for the case of small phase differences (discussed in Section 2.1 but not

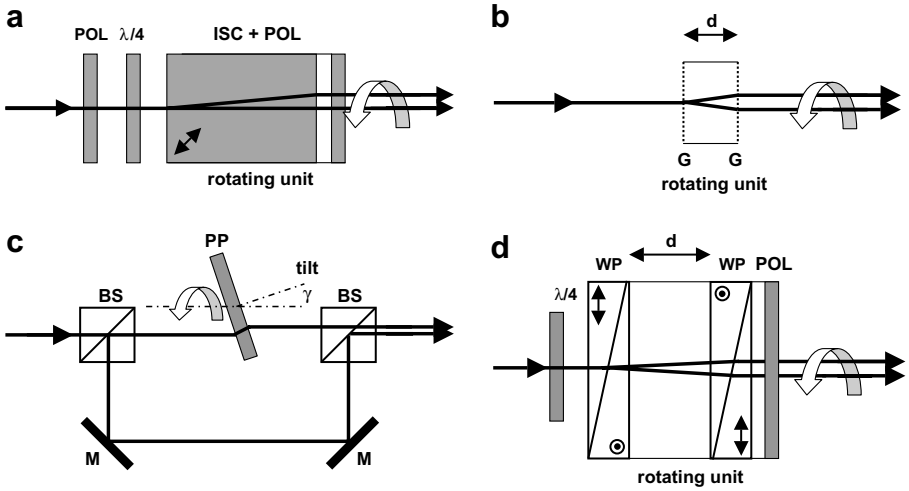

Fig. 1. Proposed designs for rotated lateral shearing devices based on (a) a birefringent image separation crystal, (b) gratings, (c) a parallel plate and (d) a pair of Wollaston prisms. The abbreviations are: POL, polariser; λ/4-quarter wave plate; G,- (Ronchi) grating; PP, parallel plate; M, mirror; WP, Wollaston prism. Following common conventions, the orientation of the ordinary axis of the birefringent crystals is indicated by double arrows or a circle with a dot in the center.

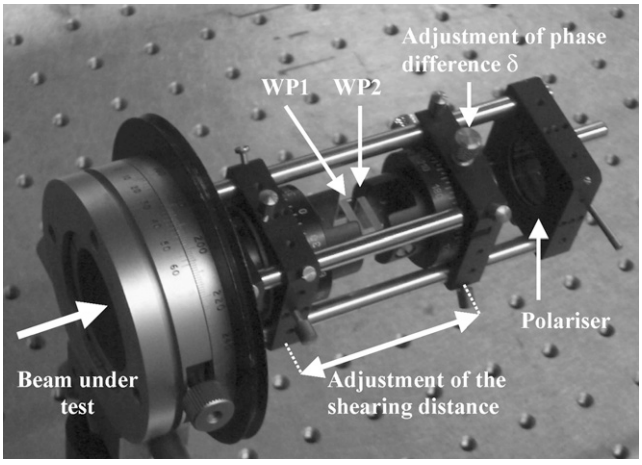

Fig. 2. Rotated lateral shearing wavefront measurement device according to the scheme shown in Fig. 1d. Two Wollaston prisms (WP1, WP2) and a polariser are combined into one rotating unit. The beam under test is circularly polarised by a quarter wave plate which is not shown.

demonstrated in this paper). Small phase differences can be accomplished by adjusting the shear distance r accordingly. Then the modulation of the detected intensity for each pixel takes a simple sinosodial waveform. It is straightforward to determine the three unknown variables amplitude, phase and background of the modulated signal by means of Fourier processing. Therefore the local wavefront slope can be reconstructed from three measurements only, even though it is again advantageous to use more measurements for the purpose of noise reduction. An investigation of the noise properties of the related Fourier processing method can be found for example in [7].

Towards the end of this paper we determine the noise in the final reconstructed wavefront for the overall process experimentally. However, the detailed interplay between the number of recorded interferograms and the error of the tilt parameter extracted as well as a direct experimental comparison between the two processing schemes will be subject of future work.

4.3. Data acquisition and image preprocessing

In a first experiment we placed a biconcave singlet lens ($f = 700$ mm) in a collimated laser beam (HeNe, 632.8 nm) and analysed the wavefront. The distance between the splitting surfaces of the Wollaston prisms was 5 mm. With the 1° total splitting angle of the Wollaston prisms this corresponds to a shearing distance of 87 μm. The beam approaching from the left is circularly polarised by a quarter wave plate (not shown). The interferograms were captured on a CCD (Pulnix PE2015) and digitised at 8-bit resolution using a framegrabber (Matrox Meteor). Pixels were also averaged over areas of 4×4 and three successive frames for the reduction of image noise. The size of the effective pixels (83 μm) was close to the shearing distance and a square region of interest with an effective number of $35 \times 35 = 1225$ intensity values was extracted from each of the interferograms.

In a second experiment, an astigmatic plastic spectacle lens was placed in the collimated beam a distance of 80 mm from the device and the wavefront was analysed under otherwise identical conditions.

4.4. Fitting procedure applied to our data

The measured intensity as a function of the shearing orientation was fitted to Eq. (7) at every effective pixel location. Fig. 3 shows an example for the fitting of one dataset to the modulated interferogram intensity. The nonlinear fitting procedure was implemented by using the

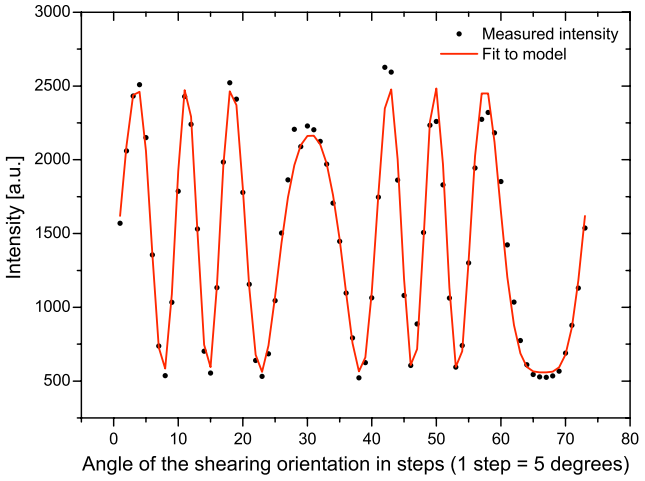

Fig. 3. Example of the fitting of the measured intensity to the analytic model, using the processing mode for arbitrary phase differences as discussed in Section 2.1.

`NonlinearRegress` command in Mathematica [16] and took approximately 4 min for the 1225 data-sets on a 2 GHz Pentium-4 PC. After the fitting the parameters $S(x,y)$ and $\alpha(x,y)$, extracted for each pixel position, are used to calculate the x/y components of the local slope of the wavefront as stated in Eq. (4).

For some inappropriate values of the starting parameters the fit did not converge. Therefore we implemented a procedure where the location of the fit within the region of interest was moved in a meander-type pattern. The fitted values from one pixel were used as the starting values for the next fit of the adjacent pixel. As a result, the very first fit needed supervision and the overall procedure was very stable. One could further automate the fitting procedure by implementing a parameter search algorithm for the very first fit, therefore obtaining a process which requires no user interaction.

Here we demonstrated fitting to the exact model (7), which is the most general case. The reader should be aware that the choice of $\delta = \pi/2$ and restrictions to small phase differences (could not be accomplished with our setup) does greatly simplify and speed up the fitting procedure. Two more data processing options (not demonstrated) were outlined in Section 2.1. Especially for the linear approximation, fast fitting procedures based on Fourier processing can be implemented.

4.5. Device calibration

The sensor was calibrated by measuring the known tilt angle (0.53°) of a collimated beam. The average of the 1225 tilt values of the dataset was used to obtain the value of the shearing distance r. With the knowledge of r the local slope of the wavefront can be calculated from the fit parameters (see Eq. (7)). Constant slope offsets were also subtracted in this step, which corresponded to a removal of the superimposed overall tilt of the measured wavefront.

Because the Wollaston prisms had slight imperfections and the alignment options were limited, the phase difference between the two sheared beams was not constant over the field of view. However, the fitting procedure, and more particularly the calculation of the slope, is not sensitive to these effects. The imperfections of the device led to a systematic error in the form of curvature (radius ≈ 1.5 m) measured for a nominally flat wavefront. In a second calibration step this systematic error was removed: a polynomial function was fitted to the data measured for a nominally flat reference wavefront. This polynomial was then subtracted from the following measurements to obtain corrected values. A subtraction of a polynomial rather than the reference function itself ensured that no additional noise was introduced during this calibration step.

4.6. Wavefront reconstruction and results

In the final stage of the procedure, the phase function itself was reconstructed from the calibrated slope measurements. Most of the vast amount of previous work on wavefront reconstruction was done in the context of the widely known Shack–Hartmann wavefront sensor [2]. The wavefront reconstruction components of the processing are compatible and can be interchanged since our sensor, like the Shack–Hartmann, detects the local slope of the wavefront. Here we reconstruct the wavefront from the slope values via direct integration: one corner of the dataset was fixed as a reference point and the value of the other points was determined by a path integral. For each point the average of the integral along two different paths was used and the procedure was repeated for all four corners. The result was the average of the four independent wavefront reconstructions. For a resolution of 35×35 phase values this took approximately 3 s in Mathematica.

The contour representation of the phase measured from the lens (nominal focal length of 700 mm) is shown in Fig. 4a, where the contours correspond to an optical path difference of 300 nm. The test lens was illuminated with a collimated beam and placed 115 mm away from the shearing device. Therefore, the curvature of the wavefront at the shearing device should correspond to 585 mm. A two-dimensional fit of the measured contour function gave a radius of 600.4 mm, equivalent to an error of 2.6%. This was within the expected range since the calibration procedure for the absolute tilt had an approximate error of 3%.

A contour plot of the result from the second experiment with the spectacle lens is depicted in Fig. 4b and fitting showed the ratio of 1.486 between the two wavefront curvatures along the main axes. This agrees well with the optician's specification of 1.5 diopters as the stronger curvature and 1 diopter in the orthogonal direction.

4.7. Noise performance

The noise performance and repeatability of the phase measurement were investigated experimentally. In the first

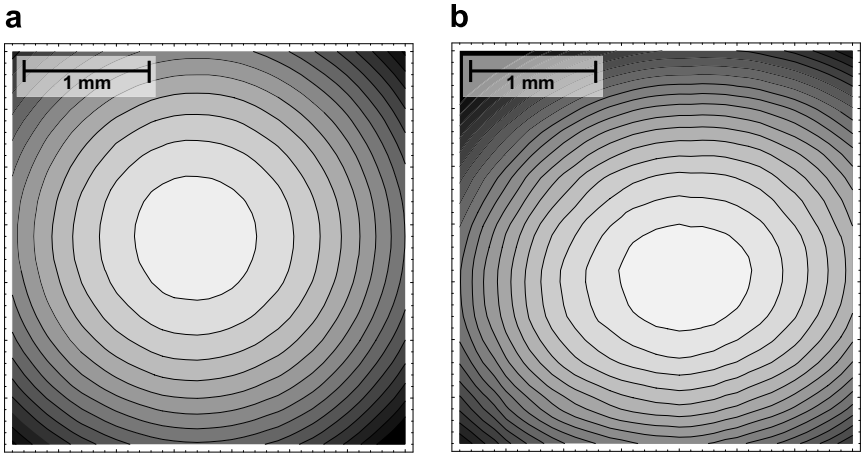

Fig. 4. Reconstructed wavefronts from two lenses. (a) $f=7\,00$ mm biconvex glass lens. The contours correspond to an in optical path difference of 300 nm. (b) Plastic astigmatic spectacle lens. The difference in curvatures along the two main axes (astigmatism) is clearly visible; the contours correspond to an optical path difference of 200 nm.

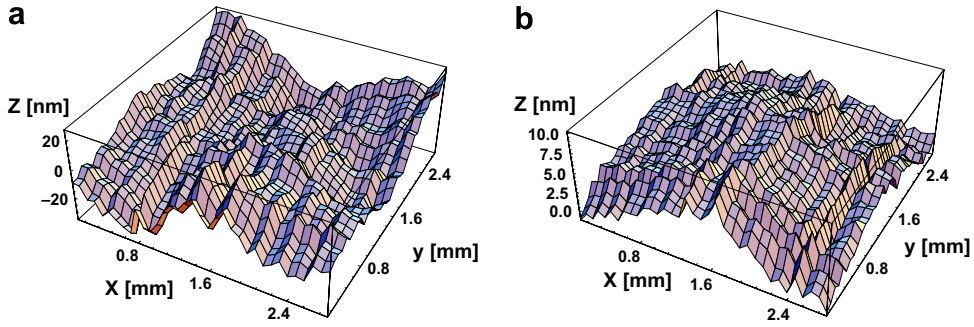

Fig. 5. Investigation of systematic errors and noise. A flat wavefront was measured twice, resulting in two measured wavefronts. (a) A second order polynomial is fitted to the first measurement and subtracted from the second measurement. The RMS value is 9.7 nm and contains systematic errors. (b) The repeatability was verified by subtracting the two subsequent wavefronts from each other. The RMS value is 2.14 nm.

step a nominally flat wavefront with superimposed tilt was measured and a second order 2D polynomial was fitted to the reconstructed wavefront. In a subsequent measurement of the same wavefront the previously obtained polynomial was subtracted. Because the measured wavefront is assumed to be continuous and smooth this procedure can reveal systematic errors without introducing additional noise from the subtraction process. Fig. 5a shows the residual data: the peak to peak value is 60 nm and the root mean square (RMS) value is 9.7 nm, corresponding to $\lambda/65$. To assess the stability of the phase measurement the two wavefronts (measured and reconstructed subsequently) were subtracted from each other and the result is shown in Fig. 5b. The peak to peak value is 11 nm and the RMS value is 2.14 nm, corresponding to $\lambda/295$ at a wavelength of 632.8 nm.

5. Summary and conclusion

We have presented a wavefront measurement technique based on rotated lateral shearing (RLS) interferometry and described the principles of measurement and data processing. Several practical implementations have been proposed. For some of the designs the dynamic sensitivity and dynamic range of the measurement can be adjusted, which is not feasible with a standard Shack–Hartmann design where the number and size of the lenslets is fixed. One of the proposed layouts uses a simple parallel plate and can be implemented at low-cost. A fundamental characteristic of this method is that the accuracy of the phase measurement does not depend on the spatial resolution of the CCD sensor because the local slope is extracted from the intensity modulation of each individual pixel. Compared to a Shack–Hartmann sensor, higher resolution spatial sampling of the wavefront slope can be obtained with a CCD of lower resolution.

A compact design based on two Wollaston prisms has been built and the required data processing and wavefront reconstruction was implemented within Mathematica. An additional important feature of the method is that we may adjust the sampling of the series $I(x,y,\theta)$ by changing the step size of the angle θ as well as the number of measurements, thus controlling the trade off between accuracy of the extracted parameters and the measurement time. Although the spatial resolution of the CCD camera determines the sampling of the wavefront we note that it does

not influence the accuracy of phase slope measurement. Only the modulation of the intensity is needed to determine the wavefront slope values for each pixel. Hence affordable low resolution CCD sensors may be used.

Compared to many other phase measurement procedures no phase stepping is required and the recovery of phase is achieved via the rotation of a single component. Even using low resolution 8-bit raw images to quantify the interferograms, the wavefront deviation from a fitted polynomial was $\lambda/65$ RMS. This figure includes systematic errors, some of which could be minimised by an improved wavefront reconstruction technique and improved quality of the optical components. The repeatability of the wavefront measurement, defined as the difference between two subsequent measurements, was found to be better than $\lambda/250$ RMS. This value is similar or better than the performance of current commercial Shack–Hartmann sensors with comparable spatial sampling of approximately 90 μm [17,18]. The spatial sampling can be easily increased to values of 400×400, using a CCD of relatively low resolution, while Shack–Hartmann sensors are typically limited to spatial sampling in the order of 128×128 and require high resolution CCD cameras.

Acknowledgements

Michael Schwertner was supported by a grant from the DAAD Germany (Deutscher Akademischer Austauschdienst) and the Basic Technology scheme of the Research Councils UK. Martin Booth is a Royal Academy of Engineering/EPSRC Research Fellow. We would like to thank the anonymous reviewer who did draw our attention to [8] and contributed the idea of processing via synchronous averaging. This work was funded by the Basic Technology scheme of the Research Councils UK and the Lubbock trust. We would like to thank Boots Opticians, High Street, Oxford for providing the astigmatic spectacle lens.

References

[1] J.H. Bruning, D.R. Heriott, J.E. Gallhager, D.P. Rosenfeld, A.D. White, D.J. Brangaccio, Appl. Opt. 13 (11) (1974) 2693.
[2] B.C. Platt, R. Shack, J. Refract. Surg. 17 (2001) 573.
[3] P. Liang, Z. Jin, C.S. Guo, H.T. Wang, Opt. Express 14 (2006) 625.
[4] J.C. Wyant, Appl. Opt. 12 (1973) 2057.
[5] M.J. Booth, M.A.A. Neil, T. Wilson, J. Opt. Soc. Am. A 19 (10) (2002) 2112.
[6] M. Takeda, H. Ina, S. Kobayashi, J. Opt. Soc. Am. 72 (1) (1982) 156.
[7] Y. Surrel, Appl. Opt. 36 (1) (1997) 271.
[8] A. Arnaud, F. Silveira, E. Frins, A. Dubra, C.D. Pericante, J.A. Ferrari, Appl. Opt. 39 (16) (2000) 2601.
[9] M. Abramowitz, I.A. Stegun, Handbook of Mathematical Functions with Formulas, Graphs, and Mathematical Tables, ninth ed., Dover Publishing, New York, 1972.
[10] A. Agrawal, R. Raskar, R. Chellappa, in: ECCV – Proceedings of the ninth European Conference on Computer Vision, Graz, Austria, 2006.
[11] F. Roddier (Ed.), Adaptive Optics in Astronomy, Cambridge University Press, 1999.
[12] P.A. Bakut, V.E. Kirakosyants, V.A. Loginov, C.J. Solomon, J.C. Dainty, Opt. Commun. 109 (1–2) (1997) 10.
[13] L.A. Poyneer, D.T. Gavel, J.M. Brase, JOSA A 19 (10) (2002) 2100.
[14] K.R. Freischlad, C.L. Koliopoulos, JOSA A 3 (11) (1986) 1852.
[15] H. Schreiber, J. Schwinder, Appl. Opt. 36 (22) (1997) 5321.
[16] Mathematica online documentation from Wolfram Research. <http://documents.wolfram.com/mathematica//>, 2006.
[17] WaveFront Sciences Inc. 14810 Central Ave. SE Albuquerque New Mexico 87123, Specifications for the CLAS-XP wavefront sensing system, <http://www.wavefrontsciences.com/CLAS-XP.pdf/>, 2006.
[18] Engineering Synthesis Design Inc. 310 South Williams Boulevard Tucson AZ, Specifications for the Intelluim H-Sense Shack Hartmann wavefront sensor, <http://www.engsynthesis.com/products_wavefront_hsense.php, 2006/>.